Propulsion and Power Research 2016;5(2):108–117

HOSTED BY

ELSEVIER

http://ppr.buaa.edu.cn/

Propulsion and Power Research

www.sciencedirect.com

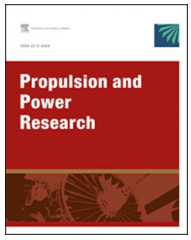

ORIGINAL ARTICLE

Influence study of flow separation on the nozzle vibration response

Geng Li*, Qin Liu, Xuequn Han, Yunqiang Guo

The 41st Institute of the Academy of China Aerospace Science and Technology Corporation, Xi'an, Shaanxi 710025, China

Received 10 April 2015; accepted 18 August 2015
Available online 24 May 2016

KEYWORDS

Solid rocket motor;
Flow separation;
Oscillation response;
Spectrum analysis;
Test engine nozzle

Abstract In the present paper, the vibration response difference of the upper stage nozzle with higher expansion ratio between ground and altitude simulation hot-firing test is analyzed. It indicates that the acceleration response of the nozzle under ground hot-firing test is much higher than that of the altitude condition. In order to find the essential reason, the experimental and numerical simulation studies of the flow separation are developed by using the test engine nozzle. The experimental data show that the nozzle internal flow occurred flow separation and the divergence cone internal wall pressure pulsation increased significantly downstream from the separation location. The numerical simulation and experimental results indicate that the increase of internal wall pressure and turbulence pulsating pressure are the substantial reason of vibration response increasing aggravatingly during the ground firing test.

1. Introduction

The increasing demand for higher performance in rocket launchers promotes the development of upper-stage nozzles with higher performance, which is achieved by increasing the expansion ratio basically. The engine like U.S.A J-2S engine, Space Shuttle sustainer Motor SSME, Russia RD-120 engine, Europe Vulcain Motor and Japan LE-7A prototype engine etc are equipped with the upper stage nozzle with higher performance in the propulsion area [1,2]. However, some launcher vehicle main stage engine will experience long periods of over-expanded operation with flow separation during ground firing testing, start-up or low altitude flight phase. Flow separation induces the dynamic load which leads to the failure of nozzle structure, even for the engine structure [3].

*Corresponding author. Tel.: +8613636717013.
E-mail address: celery@mail.nwpu.edu.cn (Geng Li).

Peer review under responsibility of National Laboratory for Aeronautics and Astronautics, China.

http://dx.doi.org/10.1016/j.jppr.2016.05.002

So in the past four decade, many studies have been developed on the occurrence of flow separation. The current literatures mainly focus on the liquid rocket motor domain. Based on the flow field theory and cold or hot flow subscale simulation test, the free shock separation, restricted shock separation and the unsymmetrical load phenomenon of separation flow are investigated comprehensively and deeply [4–8]. C.X. Huang [9] preliminarily observed a theoretical work about flow deflection which occurs during the firing test, however, the underlying physical mechanism behind separation was not totally clear. Work in the late 1990s produced the numerical simulation of CHN solid rocket motor nozzle flow separation comprehensively [10,11], but not consider the two-phase flow influence, and also was deficient in experimental validation. Y.X. Wang et al. [12] present the numerical simulation and experimental study on the separation location of the engine nozzle internal flow field during static firing test. It captured the separation critical location successfully and investigated the effect regularity of the combustion pressure and nozzle inner contour on the location. The literature review above mostly explained the flow separation phenomenon by numerical method, yet there is little work discussing the difference of wall pressure fluctuation between the upstream area and downstream region of separation point which induce the potential variation of the nozzle vibration character.

In this paper, the vibration response difference of the upper stage nozzle with higher expansion ratio between ground and altitude simulation hot-firing test is analyzed comprehensively. And a computational fluid simulation and flow fluctuation pressure experimental study of the test engine nozzle are conducted to explain and validate the essential mechanism, that is, when the flow separation occurs, the wall pressure rising and pressure impulsion amplifying, which result in the increasing of vibration amplitude of the high expansion ratio nozzle under ground hot-firing test.

2. Nozzle vibration response analysis of ground and altitude simulation static firing test

For the large expansion ratio upper stage engine, its actual working condition is nearly vacuumed ambient. So during the development process of the solid rocket motor, the altitude simulation test system is necessary to construct the approximate vacuumed ambient under sea level for the engine static firing assess test. Besides altitude simulation firing test, the sea level structure hot-firing test for the components thermal structure validation and ground joint hot-firing test for the other missile subsystem are also demand during the development process. For the limitation of the altitude simulation test system, not all the validation firing test is carried in the vacuumed cabin. So need to be explained here, the ground static firing test has its specific validate purpose and it can not simulate the real working condition absolutely, but the estimate of nozzle components thermal protection and structure strength can be validated entirety.

In this section, the contrast analysis of the vibration data of the upper stage nozzle exit cone under ground and altitude simulation static firing test is carried out particularly.

2.1. Time-domain analysis

The vibration test point is located on the nozzle exit cone supporting lug. Figure 1(a) and Figure 1(b) present the measuring point acceleration versus time curves of the altitude and ground firing test respectively. It indicates that the acceleration amplitude of ground testing is from 50 g to 50 g, while the data of altitude simulation testing is only from 6 g to 6 g, the vibration amplitude of the ground test is much higher than that of altitude test.

Table 1 gives the acceleration information of ground and altitude simulation test. From the data above, it can be seen that the maximum, minimum, peak-to-peak value, RMS and the stand deviation which produced under ground firing test are far greater than that of altitude condition, that's mean,

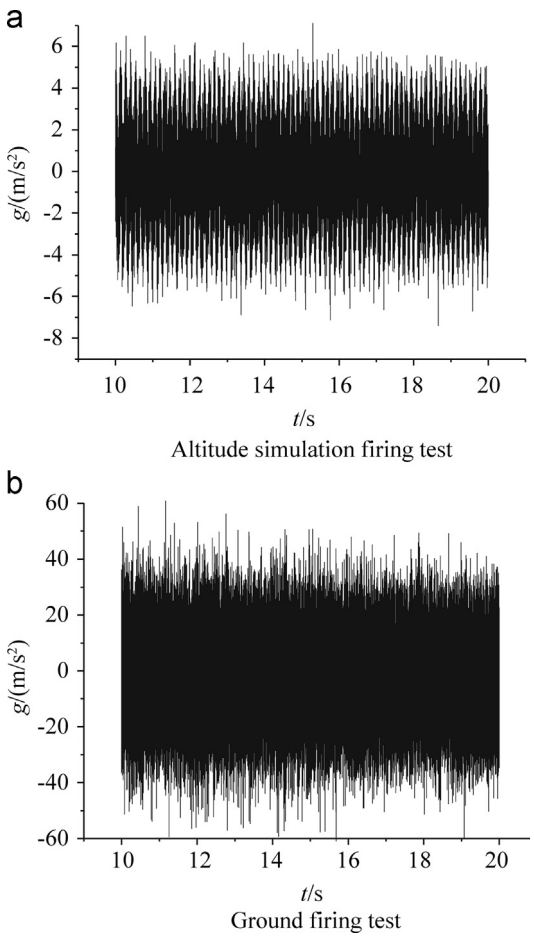

Figure 1 Acceleration vs. time curve. (a) Altitude simulation firing test and (b) ground firing test.

the vibration amplitude, power and fluctuation level of ground test are rather severely.

2.2. *Frequency-domain analysis*

In this section, the frequency-domain analysis is developed by the acceleration to obtain the nozzle vibration characteristics. The FFT method is used to transform the time domain signal. Figure 2 presents the vibration acceleration spectrum of the altitude simulation testing and the ground firing testing condition. It indicates that for the response amplitude there is great difference between altitude and ground firing testing. The maximum acceleration response spectrum amplitude under altitude simulation test is approximately 0.0985 m/s^2, while the maximum amplitude of the ground firing is up to 1.173 m/s^2 and it is much larger than that of the altitude one.

In addition, from Figure 2 it also can be seen that there are some specific predominant peak frequency information in the acceleration spectrum. Table 2 lists these corresponding frequencies, and Table 3 gives the test modal parameters of the nozzle. From the comparison of these modal parameters it can be indicates that these frequencies are very close to the nozzle modal frequency.

Table 1 Acceleration peak-to-peak value.

Test ambient	Altitude	Ground
Max	7.11	67.93
Min	−7.40	−63.30
Peak-to-peak	14.51	131.23
Mean square root	1.758	14.391
Standard deviation	1.743	13.741

Table 2 Peak value.

No.	Predominant peak frequency/Hz	
	Altitude	Ground
1	15.3	15.3
2	30.5	31.7
3	60.4	63.5
4	/	95.8

Table 3 Modal parameters.

Order	Frequency/Hz	Mode shape
1	18.90	Swing deformation
2	34.00	Twisting deformation
3	64.14	Ellipse deformation
4	95.96	Triangular deformation

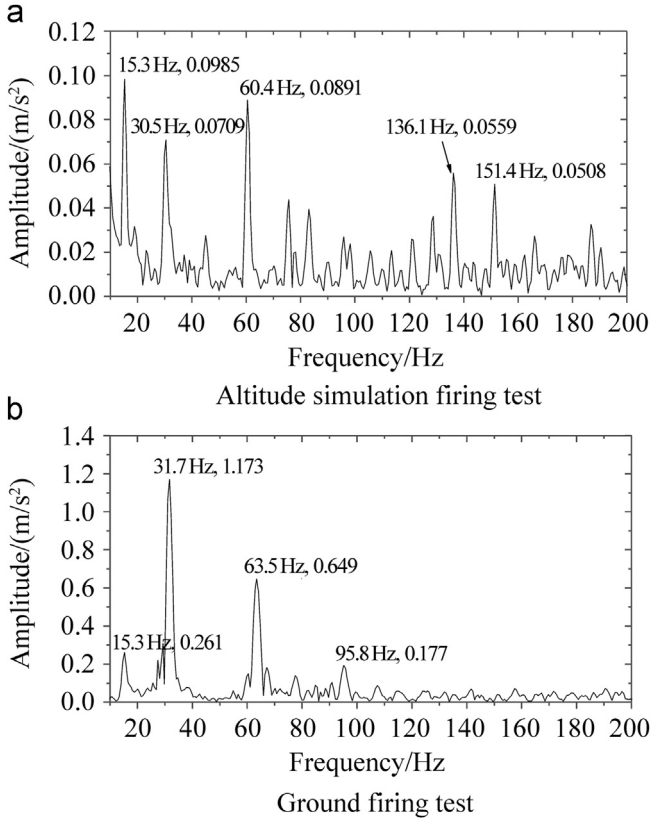

Figure 2 Vibration acceleration spectrum. (a) Altitude simulation firing test and (b) ground firing test.

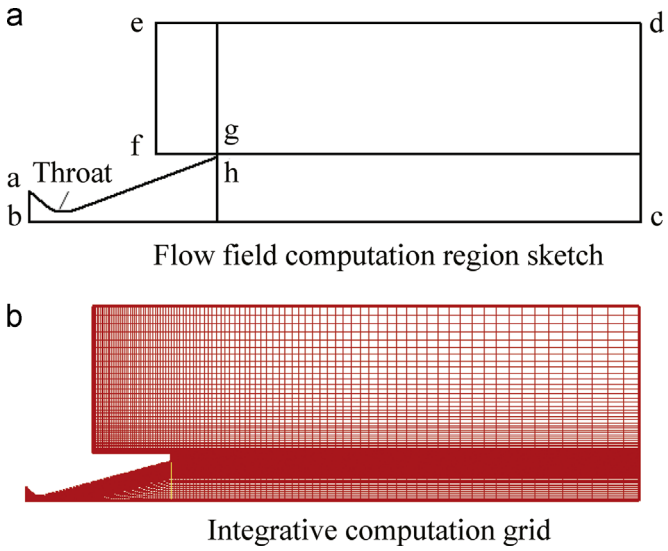

Figure 3 Computational fluid dynamics (CFD) model. (a) Flow field computation region sketch and (b) integrative computation grid.

The above frequency domain analysis shows that the difference of vibration characteristics of the nozzle between ground and altitude simulation hot-firing test is obviously. The vibration acceleration of the ground firing test is much higher than that of the altitude condition. These data information are very similar with that of the time domain analysis.

The wider fluctuation margin of vibration response implied that there is different excitation resource for the test engine nozzle under different test condition. It indicates that compare to the approximate vacuum ambient, the local ambient pressure influence on the internal flow field is possibly the essential reason that induced the variety of vibration response.

3. Internal flow field comparison analysis

In this section, the internal flow comparison analysis of nozzle structure under ground and altitude simulation firing test condition is developed by the simulation method. The ambient pressure of the ground and altitude simulation condition is about 94 kPa and 10 kPa respectively. And it will affect the flow character significantly.

3.1. Modeling and meshing

Figure 3 describes the 2D axisymmetric flow field computation region and its integrative computation grid of the test motor nozzle model. Here, the diameter of the nozzle throat is Φ20 mm, the expansion ratio is 72, and the convergent semi-angle and the expansion semi-angle are 40° and 15° respectively. The integrative computation grid technique is used to simulate the nozzle structure and its outfield flow field. And the computational domain extends up to 10 times nozzle exit diameters from the axis and 5 times exit diameters from the radial direction. The wall mesh density is refined and adjusted in order to capture the separation point location (Figure 3(b)).

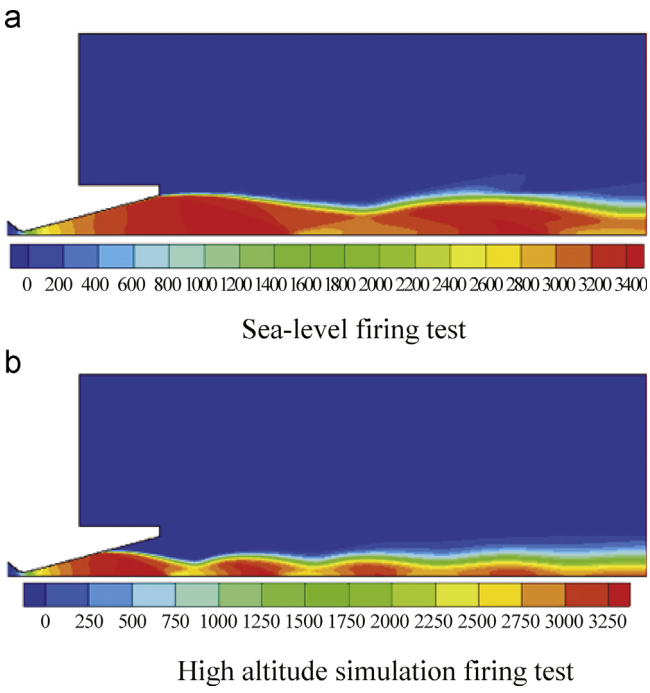

Figure 4 Velocity distribution. (a) Sea-level firing test and (b) high altitude simulation firing test.

3.2. Boundary condition

The nozzle entrance pressure is the entrance boundary condition and the flow direction is vertical to entrance direction, gas total temperature, pressure and entrance

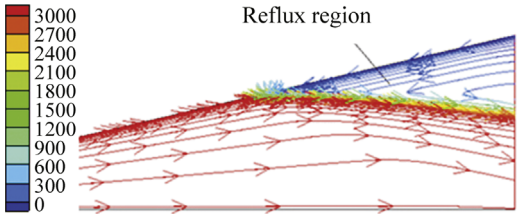

Figure 5 Velocity streamlines distribution of the separated flow field reflux region.

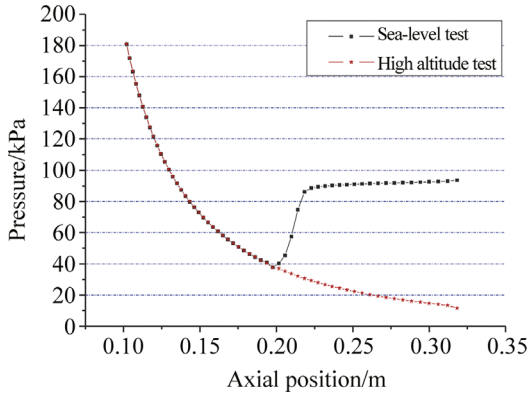

Figure 6 Comparison of wall pressure distribution curve.

turbulent parameter, bc stand for the axes, axisymmetric boundary condition, ah,hg and gf are the diathermic wall without sliding. ef and ed are the pressure far-field boundary condition. The gas parameter is obtained by the heating calculation and the far-field atmosphere attribute property is obtained by normal condition

3.3. Numerical method

For separation flow causes shock wave, and it includes the transportation of hot gas and air components. In this section, the Cell-Centered Finite Volume Method is developed to solve the Navier-Stokes equations which based on the conservation of density. In order to obtain more precise results, the convective term is discretized using the AUSM (advection upstream splitting method) and approximated by the MUSCL (monotone upstream-centered scheme for conservation laws). *K*-ω SST (shear stress transport) two-equation vorticity viscous model is employed for the turbulent model. Wilcox *K*-ω model is presented near the wall and *K*-ω model is adopted in the mean flow. A blend functions is present here to realize the transition. Wall functions were used near the wall. The molecular viscosity is expressed in the following form of Sutherland law:

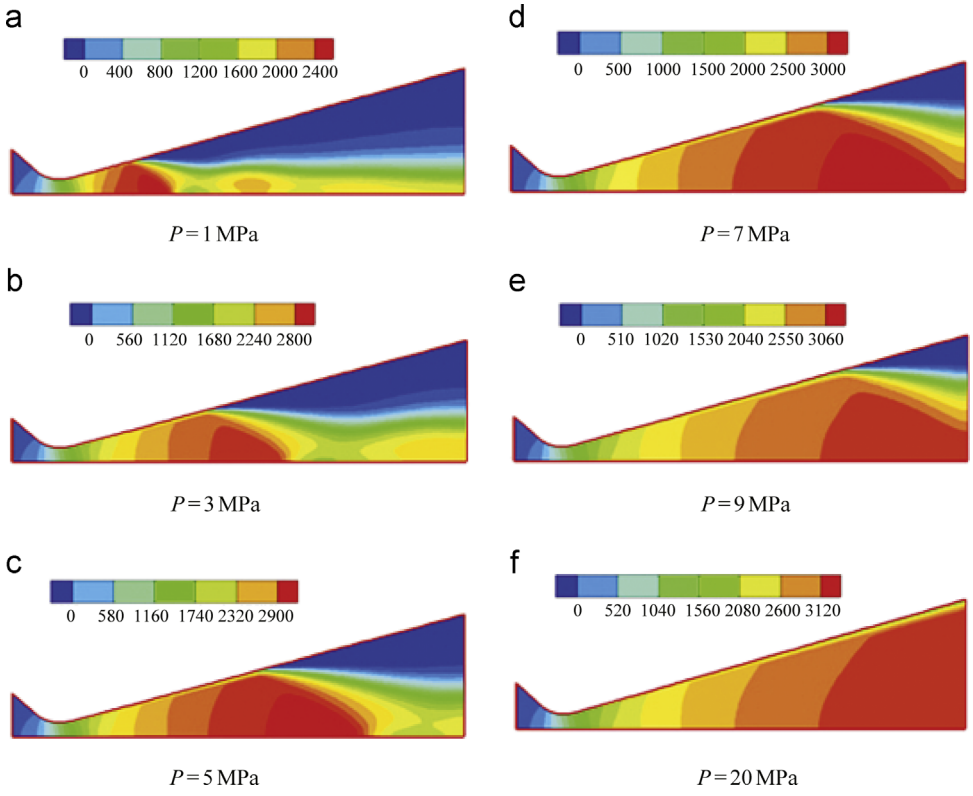

Figure 7 Velocity distribution of internal flow field at different pressure. (a) $P=1$ MPa, (b) $P=3$ MPa, (c) $P=5$ MPa, (d) $P=7$ MPa, (e) $P=9$ MPa, (f) $P=20$ MPa.

$$\mu = \mu_0 \left(\frac{T}{T_0}\right)^{3/2} \frac{T_0+S}{T+S}$$

where, the reference temperature $T_0 = 273.5$ K, the equivalent temperature $S = 110.56$ K, the reference viscous coefficient $\mu_0 = 1.716 \times 10^{-5}$ kg/(m·s)

3.4. Numerical results

Figure 4 gives the velocity distribution of the test motor nozzle flow field under different working condition. Compare to the Figure 4(a) and Figure 4(b) it can be seen that the nozzle internal flow field is full flow status when it under high altitude simulation firing test, while when it operating the sea-level firing test, the internal flow field of the nozzle present overexpanded pattern, the flow separation appeared obviously. An oblique shock occurs near the separation point location and intersects at the nozzle exit. The reflux region with low velocity is formed downstream from the separation location (Figure 5).

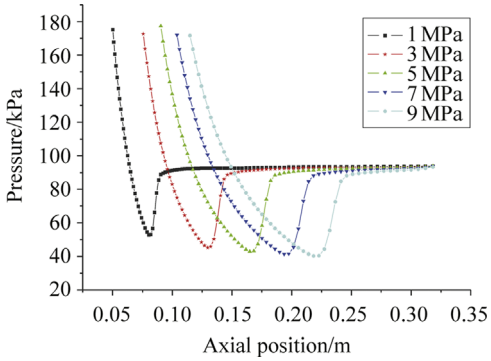

Figure 8 Wall pressure distribution of internal flow field on different pressure.

Figure 6 presents the wall pressure distribution of the nozzle under different testing condition. It illustrates that the wall pressure of the nozzle structure monotone decreasing along the axial direction under full flow status, while the wall pressure will increase severely at the separation location and then the pressure is close to the ambient pressure at the nozzle exit. The numerical simulation shows that the expansion ratio and pressure of the separation point are 26.5 kPa and 35 kPa respectively.

The velocity distribution of the nozzle internal flow field under different combustion chamber pressure is given in Figure 7. It shows that the chamber pressure affect the position of the separation point significantly. When the chamber with low pressure, the separation location is near to the nozzle entrance, the oblique shock intersects at the inner the nozzle, meanwhile the continuous compression expansion waves system is formed. With the chamber pressure increasing, the separation point will move to the nozzle entrance and the intersect location also will shift to the outside of the nozzle exit gradually. The nozzle internal flow field will present full flow pattern if the chamber pressure is high enough.

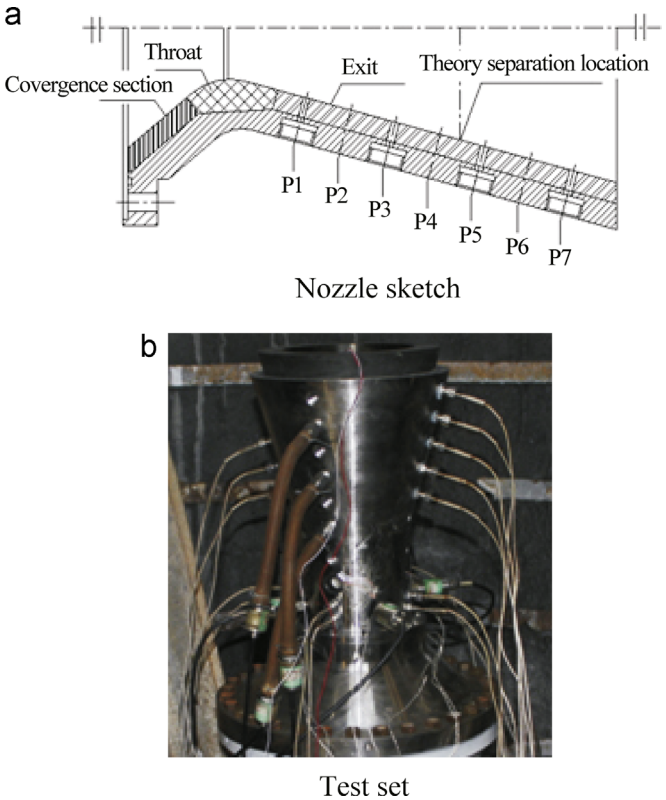

Figure 9 Test nozzle apparatus. (a) Nozzle sketch and (b) test set.

Figure 8 describes the wall pressure distribution of the nozzle internal flow field vs. pressure. It indicates that with the pressure increasing, the separation pressure decreases and the separation point shifts to the nozzle exit gradually at a constant ambient pressure. This is because that the fluid near to the nozzle wall boundary layer is subsonic speed due to the viscosity effect, so the ambient pressure has no effect on the nozzle internal flow field when the nozzle is in underexpanded or full expanded condition. While when the nozzle is in the overexpanded pattern, there is a possibility that the internal flow field will be influenced by the external disturbance. When the kinetic energy of the boundary layer airstream is deficiency enough to overcome the pressure gradient behind shock, the flow separation is occurred. And also the higher the working pressure is, the larger the gas velocity speed is, that's mean the ambient pressure need to overcome the larger flow kinetic energy that it can lead to the flow separation. While the ambient pressure is constant, so the closer to the nozzle exit is, the lower the wall pressure of the separation point is.

4. Flow separation experimental investigation

In this section, the separation flow test is designed to investigate the internal relation between the pulsating pressure and separated flow field by using the simulation test solid rocket motor.

4.1. Experimental programme

The flow simulation results indicates that nozzle internal flow field will take on full flow condition during the high altitude simulation firing test while separating during the ground firing test just because of the difference of the ambient pressure. When the flow separation occur the inner wall pressure downstream the separation point increases sharply and close to the ambient pressure. So the objective of the present experiment is to capture the separation point position and obtain the level of pulsating pressure.

Figure 9(a) gives the sketch of separated flow field test nozzle. The Φ4 mm pressure tapping hole vertical to the inner wall and the sensor install interface are processed on the nozzle exit cone. The sealing gasket is copper material. Pressure test points are distributed bus-bar arrangement along the nozzle divergence section. The pressure sensor range of test points P1 is 1 MPa range and negative pressure sensors are selected for test points P2 to P7 according to the prediction of internal flow field numerical simulation analysis. The test motor chamber average pressure is 7.05 MPa and working time is 20.39 s. Figure 9(b) shows the test motor nozzle prototype which prepared for the ground firing test.

4.2. Experimental results analysis

Figure 10 presents the tested nozzle photograph during and after the ground firing test. It indicates that there is an obvious erosion boundary appears on the insulation of the exit cone inner wall and the ablation condition is different visibly. The test gain insight into the flow separation information successfully.

Figure 11 describes the pressure versus time curves of test points P1 to P7. From the pressure variety of these points it can be seen that the wall pressure decreased gradually along the axial direction from point P1 to P4, the average pressure reduced from 0.6 MPa to 32.5 kPa, while for the point P5, the pressure is increased to 90.0 kPa accidentally, and then the pressure of test points P6 and P7 enhance to 92.0 kPa and 93.4 kPa respectively, which is very close to the ambient pressure 94 kPa.

Figure 12 compares the numerical and experimental results of wall pressure distribution along axial direction. It shows that the test pressures are in good agreement with the numerical results only the experimental pressure upstream the separation point is less than the numerical one appreciably. This is because of the energy loss during the flow process. The expansion ratio of the numerical separation position is 26.5, while

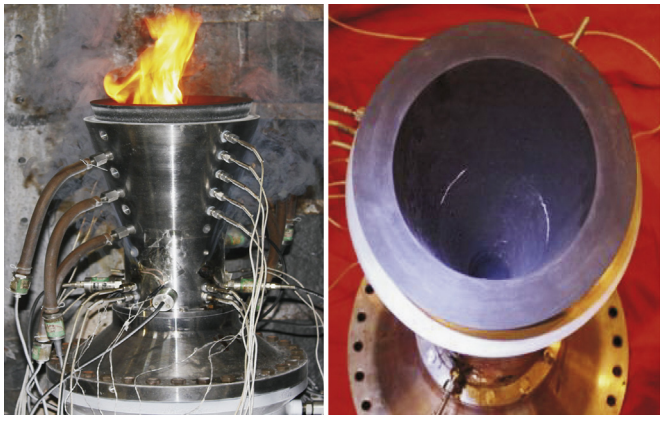

Figure 10 Photograph of tested nozzle during/after ground hot firing test.

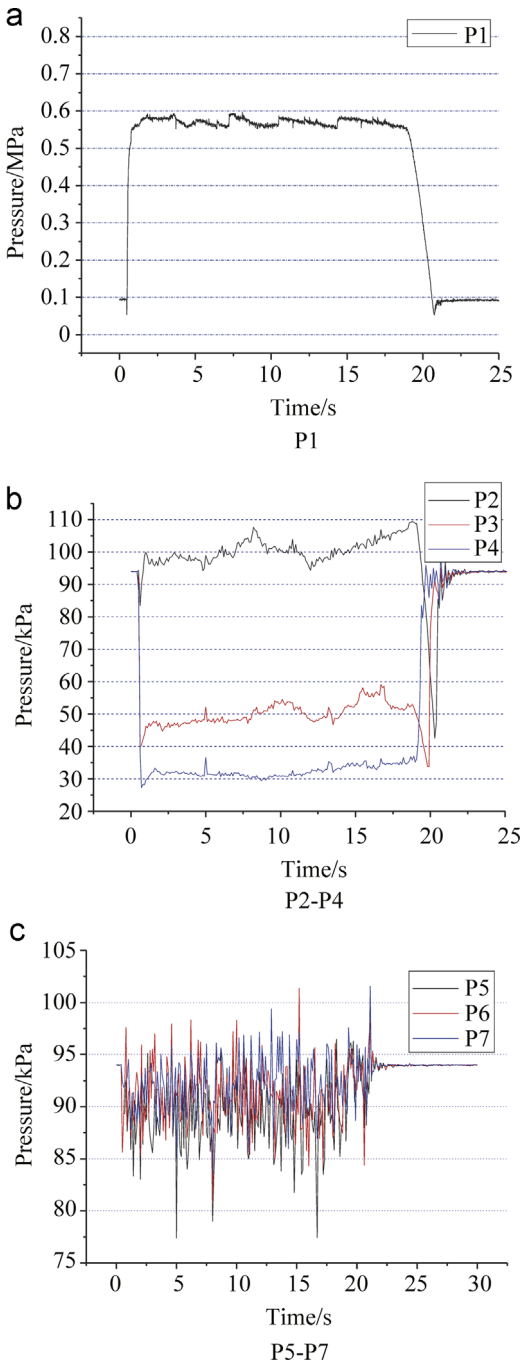

Figure 11 Pressure-time curve of the test points P1-P7. (a) P1, (b) P2-P4, and (c) P5-P7.

the test wall pressure varies significantly between test points P4 and P5 (the corresponding expansion ratio is 24 and 30 respectively), at the same time, the erosion boundary on the insulation of the exit cone inner wall is also between P4 to P5, that's mean the separation location of the test nozzle is between the two points obviously and the test capture the flow separation information accurately.

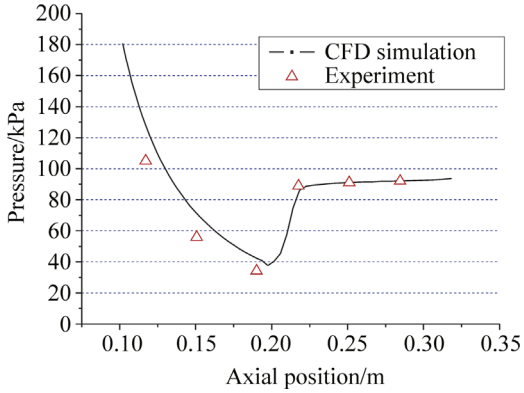

Figure 12 Comparison of computational and testing wall pressure.

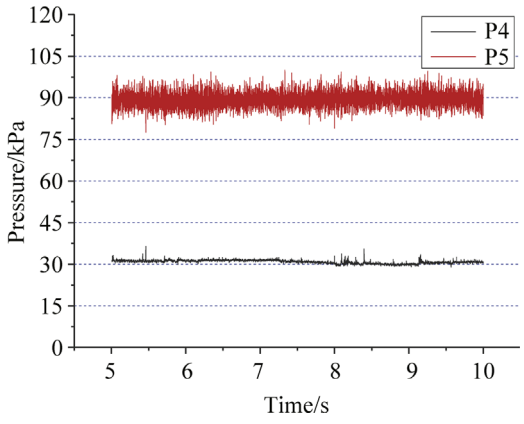

Figure 13 Pressure vs. time curve of P4 and P5.

Figure 13 presents the comparison curve of pressure versus time of the test points P4 and P5. It shows that the real pressure pulse is great different at upstream and downstream separation location. The pulsating pressure is stable upstream the separation position and the amplitude is about 2 kPa, when the separation appears the pulse pressure become unstable and the pulse amplitude is up to 15 kPa.

Figure 14 gives the pressure spectrum of the point P4 and P5. It also indicates the amplitude of the pressure pulsation downstream the separation position is up to 0.183 kPa, which is much larger than that of the separation upstream location (the maximum amplitude is not exceed 0.0283 kPa). Also a statistic analysis of P4 and P5 pressure parameter is developed in Table 4. The peak of pressure is 7.62 kPa upstream the separation location and is 22.55 kPa downstream the separation point.

The above experimental pressure information analysis of time domain and frequency domains shows that when the flow separation occurs, the pressure downstream the separation location will increase significantly and the pressure pulse of the nozzle inner wall also enhanced sharply. It will produce larger motivate load to the exit cone and lead to the vibration destruction of the nozzle structure.

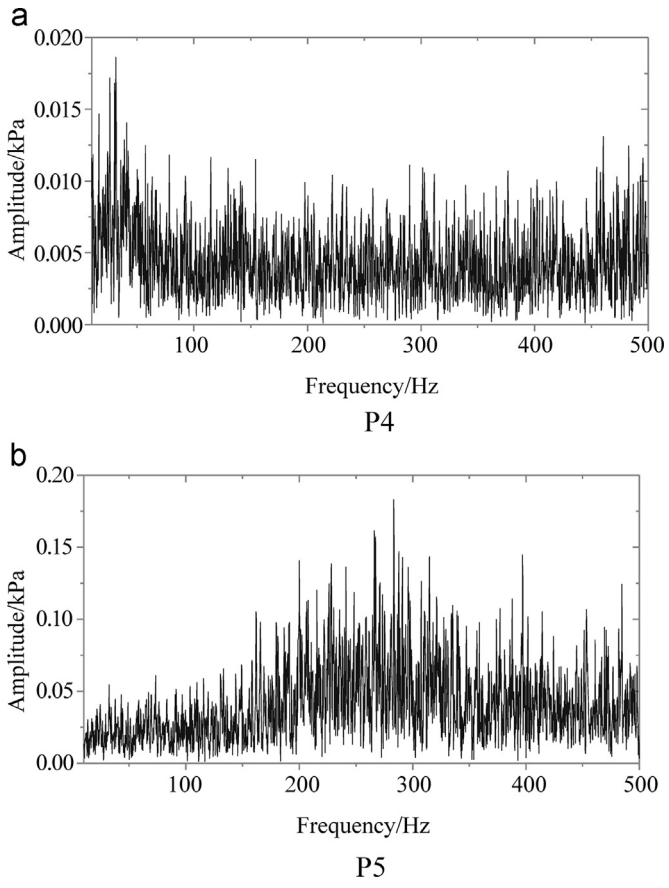

Figure 14 Pressure spectrum of test points. (a) P4 and (b) P5.

Table 4 Statistic analysis of pressure of test point P4-P5.

Test point	P_{Min}/kPa	P_{Max}/kPa	Peak-to-peak/kPa	Standard deviation
P4	28.91	36.53	7.62	0.635
P5	77.49	100.04	22.55	2.929

5. Conclusions

In the present study, the difference of vibration response of the upper stage larger expansion ratio nozzle between ground and altitude simulation hot-firing test is first being found and analyzed, it shows that the vibration acceleration response of the ground firing test is much higher than that of the altitude condition. Meanwhile there is some specific predominant peak frequency information in the acceleration spectrum and these frequencies are very close to the nozzle modal frequency. In order to investigate the essence of the phenomena, the experimental and numerical simulation studies of the flow separation are studied by using the test engine nozzle. The results indicate that the flow separation of the nozzle with larger expansion ratio will occur during the ground static firing test process because of the ambient pressure influence. The separation point will move to the nozzle exit and its pressure will reduced when the chamber pressure enhanced. The characteristics of the pulsating pressure upstream and downstream the separation location is distinct, the pressure downstream the separation point increased sharply and the pulse amplitude enhanced significantly. Flow separation will produce larger motivate load to the exit cone and cause the vibration destruction of the nozzle structure. This is the substantial reason that the vibration response produced during the ground firing test is much larger than that of the high altitude firing test.

These conclusions instruct the nozzle designer to consider the test environment influence on the large expansion ratio upper stage engine nozzle design, it can avoid the test failure occur during the ground firing test process and promote the design proposal feasibility assessment during the engine development process.

Acknowledgements

The authors would like to thank for the supports by National Basic Research Development Program of China (973-613184 Project)

References

[1] A. Hadjadj, M. Onofri, Nozzle flow separation, Shock. Waves 19 (2009) 163–169.

[2] G. Hagemann, M. Frey, Shock pattern in the plume of rocket nozzles: needs for design consideration, Shock. Waves 17 (6) (2008) 387–395.

[3] K. Smalley, A.M. Brown, J. Ruf, J. Gilbert, Flow separation side loads excitation of rocket nozzle FEM, AIAA 2007–2242, 2007.

[4] J. Östlund, Flow processes in rocket engine nozzles with focus on flow separation and side-loads, Technical Report, 2002, 09.

[5] M. Terhardt, G.I. Hagemann, M. Frey, Flow separation and side-load, Behaviok of the Vulcain engine AIAA 99-31448, 1999.

[6] T. Tomita, H. Sakamoto, Sub-scale nozzle combustion tests of the LE-7A engine for clarification of large side-loads, I: formation of RSS structure due to combustion condition AIAA 2002-3842, 2002.

[7] T.S. Wang, Transient three-dimensional analysis of side load in liquid rocket engine nozzles AIAA 2004-3681, 2004.

[8] L.H. Nave, G.A. Coffey, Sea-level side loads in high-area-ratio rocket engines, AIAA Paper 73-1284, 1973.

[9] C.X. Huang, Flame swing analysis of the nozzle under high altitude hot-firing test, Journal. Astronaut. 4 (1988) 1–9.

[10] L.Q. Chen, X. Hou, Separation flow simulation investigation on the solid rocket nozzle, Journal. Solid Rocket. Technol. 19 (1) (1996).

[11] D.C. Sun, J. Li, T.M. Cai, Numerical simulation of flow separation in nozzle, Propulsion, Technology 20 (6) (1999) 19–21.

[12] Y.J. Wang, F.T. Bao, J.J. Du, Numerical simulation and experiment of flow separation in SRM nozzle, Journal. Solid Rocket. Technol. 33 (4) (2010) 406–408.